Available online at www.sciencedirect.com
SCIENCE DIRECT®
Electric Power Systems Research 68 (2004) 61–74
ELECTRIC POWER SYSTEMS RESEARCH
www.elsevier.com/locate/epsr

Robust STATCOM voltage controller design using loop-shaping technique

A.H.M.A. Rahim *, M.F. Kandlawala

Department of Electrical Engineering, KF University of Petroleum and Minerals (KFUPM), P.O. Box 349, Dhahran 31261, Saudi Arabia

Received 22 July 2002; received in revised form 9 January 2003; accepted 5 May 2003

Abstract

Static synchronous compensator (STATCOM) is a shunt-connected converter, which can affect rapid control of reactive flow in the transmission line by controlling the generated a.c. voltage. This article presents a robust STATCOM voltage controller design for power system damping. The method of multiplicative uncertainty has been employed to model the variations of the operating points. The design is carried out applying robustness criteria for stability and performance. A loop-shaping technique has been employed to select a suitable open-loop transfer function, from which the robust controller function is constructed. The controller was tested for a number of disturbances including three-phase fault. The damping provided by the robust controller was compared with a fixed-parameter PID controller, whose gains were calculated through a pole-placement technique. It has been observed that the PID control is ineffective at operating points other than nominal. The robust design has been demonstrated to provide extremely good damping characteristics over a range of operating conditions.

Keywords: STATCOM; Shunt-connected FACTS; Damping control; Robust control; Loop-shaping technique; Pole-placement

1. Introduction

Fast acting solid state, thyristor switches of the FACTS devices are known to improve both the transient as well as dynamic performance of a power system [1]. Fixed or mechanically switched capacitors and reactors have long been employed to increase the steady-state power transmission by controlling the voltage profile along the lines. Controllable synchronous voltage sources known as static compensators are a recent introduction in power system for dynamic compensation and for real time control of power flow. The static synchronous compensator (STATCOM) provides shunt compensation in a way similar to the static var compensators (SVC), but utilizes a voltage source converter rather than shunt capacitors and reactors [2,3]. STATCOM is an active device, which can control voltage magnitude and, to a small extent, the phase angle in a very short time and, therefore, has the ability to improve the system damping as well as voltage profiles of the system. It has been reported that STATCOM can offer a number of performance advantages for reactive power control applications over the conventional SVC because of its greater reactive current output at depressed voltage, faster response, better control stability, lower harmonics and smaller size, etc. [4]

The STATCOM is normally designed to provide fast voltage control and to enhance damping of inter-area oscillations. A typical method to meet these requirements is to superimpose a supplementary damping controller upon the automatic voltage control loop [4]. Several recent articles have reported that STATCOM can provide damping to a power system [5,7–10]. They have also been shown to improve torsional oscillations in a power system [11].

Two basic controls are implemented in a STATCOM. The first is the a.c. voltage regulation of the power system, which is realized by controlling the reactive power interchange between the STATCOM and the power system. The other is the control of the d.c. voltage

* Corresponding author. Tel.: +966-3-860-2277; fax: +966-3-860-3535.
E-mail address: ahrahim@kfupm.edu.sa (A.H.M.A. Rahim).

0378-7796/03/$ - see front matter © 2003 Elsevier B.V. All rights reserved.
doi:10.1016/S0378-7796(03)00153-6

across the capacitor, through which the active power injection from the STATCOM to the power system is controlled [5,6]. PI controllers have been found to provide stabilizing controls when the a.c. and d.c. regulators were designed independently. However, joint operations of the two have been reported to lead to system instability because of the interaction of the two controllers [6,8,12]. While superimposing the damping controller on the a.c. regulator can circumvent the negative interaction problem, the fixed parameter PI controllers have been found invalid, or even to provide negative damping for certain system parameters and loading conditions [4]. Application of control that performed over a range of operating conditions has also been reported in recent times. Farasangi and Chen proposed a robust controller for SVC and STATCOM devices using H_∞ techniques and direct feedback linearization, respectively [13,14]. These designs are often complicated restricting their realization. A robust design for a current-controlled STATCOM was presented in [15] considering a simplified reduced order power system model.

This article presents a simple graphical loop-shaping technique for designing a robust damping controller for a STATCOM. A detailed power system model was considered. Two controls were identified with the voltage controlled STATCOM—the voltage magnitude and its phase angle. Robust stability and performance measures were employed to derive a constant-coefficient robust voltage magnitude controller function in the s-domain. The proposed controller was tested over a range of operating conditions for a number of disturbances and was found to provide good damping characteristics.

2. The system model

A single machine infinite bus system with a STATCOM installed at the mid-point of the transmission line is shown in Fig. 1. The system consists of a step down transformer (SDT) with a leakage reactance X_{SDT}, a three phase GTO-based voltage source converter, and a d.c. capacitor. The STATCOM is modeled as a voltage sourced converter (VSC) behind a SDT. The VSC generates a controllable a.c. voltage source $V_0(t) = V_0 \sin(\omega t - \psi)$ behind the leakage reactance. Depending on the magnitude of V_0, current I_{Lo} can be made to lead or lag the bus voltage V_L. Thus the STATCOM can be made to supply or absorb reactive power by controlling the voltage magnitude of the VSC. Generally, the STATCOM voltage is in phase with the bus voltage. However, some active power control may be possible through a limited control of phase angle ψ. This would necessitate a power source behind the capacitor voltage. The dynamic relation between the capacitor voltage and

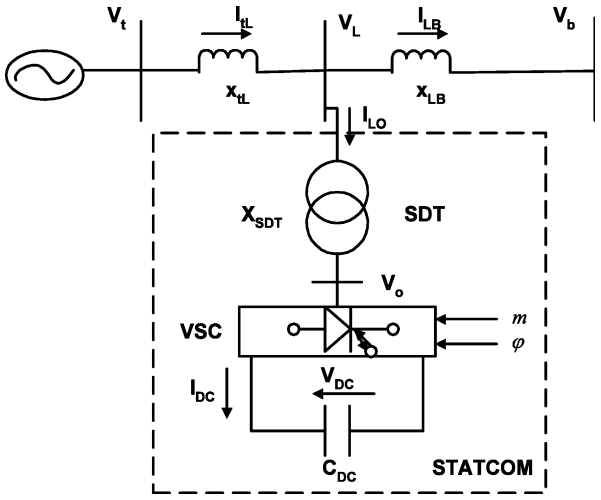

Fig. 1. The single machine infinite bus power system with STATCOM.

current in the STATCOM circuit are expressed as [6,8],

$$\frac{dV_{dc}}{dt} = \frac{I_{dc}}{C_{dc}} = \frac{m}{C_{dc}}(I_{Lod}\cos\psi + I_{Loq}\sin\psi) \tag{1}$$

where, I_{Lod} and I_{Loq} are the direct and quadrature axes components of STATCOM current I_{Lo}. The output voltage phasor is

$$\bar{V}_0 = mV_{dc}\angle\psi \tag{2}$$

The magnitude of the STATCOM voltage depends on m, which is a product of the a.c./d.c. voltage ratio and the modulation ratio defined by the PWM.

The dynamics of the generator and the excitation system are expressed through a fourth order model given as

$$\begin{aligned}
\dot{\delta} &= \omega - \omega_0 \\
\dot{\omega} &= -\frac{1}{M}[P_m - P_e - D(\omega - \omega_0)] \\
\dot{e}'_q &= \frac{1}{T'_{do}}[E_{fd} - e_q] \\
\dot{E}_{fd} &= -\frac{1}{T_A}(E_{fd} - E_{fdo}) + \frac{K_A}{T_A}(V_{to} - V_t)
\end{aligned} \tag{3}$$

A list of symbols is given in the Appendix A. The expressions for the power output, terminal voltage, and the d–q axes currents in the transmission line and STATCOM, respectively, are

$$
\begin{aligned}
P_e &= V_d I_{tLd} + V_q I_{tLq} = e'_q I_{tLd} + (x_d - x'_d) I_{tLq} \\
V_t &= \sqrt{V_d^2 + V_q^2} = \sqrt{(e'_q - x'_d I_{tLd})^2 + x'_q I_{tLq}^2} \\
I_{tLd} &= \frac{\left(1 + \frac{X_{LB}}{X_{SDT}}\right) e'_q - \frac{X_{LB}}{X_{SDT}} m V_{dc} \sin\psi - V_b \cos\delta}{X_{tL} + X_{LB} + \frac{X_{TL}}{X_{LB}} + \left(1 + \frac{X_{LB}}{X_{SDT}}\right) x'_d} \\
I_{tLq} &= \frac{\frac{X_{LB}}{X_{SDT}} m V_{dc} \cos\psi + V_b \sin\delta}{X_{tL} + X_{LB} + \frac{X_{TL}}{X_{LB}} + \left(1 + \frac{X_{LB}}{X_{SDT}}\right) x'_q} \\
I_{Lod} &= \frac{e'_q}{X_{SDT}} - \frac{(x'_d + X_{tL}) I_{tLq}}{X_{SDT}} - \frac{m V_{dc} \sin\psi}{X_{SDT}} \\
I_{Loq} &= \frac{m V_{dc} \cos\psi}{X_{SDT}} - \frac{(x'_d + X_{tL}) I_{tLq}}{X_{SDT}} \\
\Delta e_q &= \Delta e'_q + (x_d - x'_d) \Delta I_{tLd}
\end{aligned}
\tag{4}
$$

For a choice of the state and control vectors as $[\Delta\delta \quad \Delta\omega \quad \Delta e'_q \quad \Delta E_{fd} \quad \Delta V_{dc}]^T$ and $[\Delta m \quad \Delta\psi]^T$, respectively, the nonlinear state model Eqs. (1) and (4) for the generator—STATCOM system can be expressed as [8]

$$\dot{x} = f(x, \ u) \tag{5}$$

The linearized state model for small perturbation around a nominal operating condition is expressed as

$$
\begin{aligned}
\dot{x} &= Ax + Bu \\
y &= Hx
\end{aligned}
\tag{6}
$$

Here, H represents the relation between the perturbed state vector x and the chosen output y. Fig. 2 shows the block diagram for the linearized system. The derivations for the linearized system are included in Appendix B.

3. Robust control design

The damping control problem for the nonlinear power system model is stated as: given the set of equations (5), design a controller whose output u will stabilize the system following a perturbation. Since there is no general method of designing a stabilizing controller for the nonlinear system, one way would be to perform the control design for a linearized system; the linearization being carried out around a nominal operating condition. If the controller designed is 'robust' enough to perform well for the other operating conditions in the vicinity, the design objectives are met.

The changes in operating points of the nonlinear system can be considered as perturbations in the coefficients of the linearized system matrices. These perturbations are modeled as multiplicative uncertainties and robust design procedure is applied to the perturbed linear systems. This section gives a brief theory of the uncertainty model, the robust stability criterion, and a graphical design technique termed loop shaping, which is employed to design the robust controller. Finally, the algorithm for the control design is presented.

3.1. Uncertainty modeling

Suppose that a plant having a nominal transfer function P belongs to a bounded set of transfer functions $\mathscr{P}$. Consider that the perturbed transfer

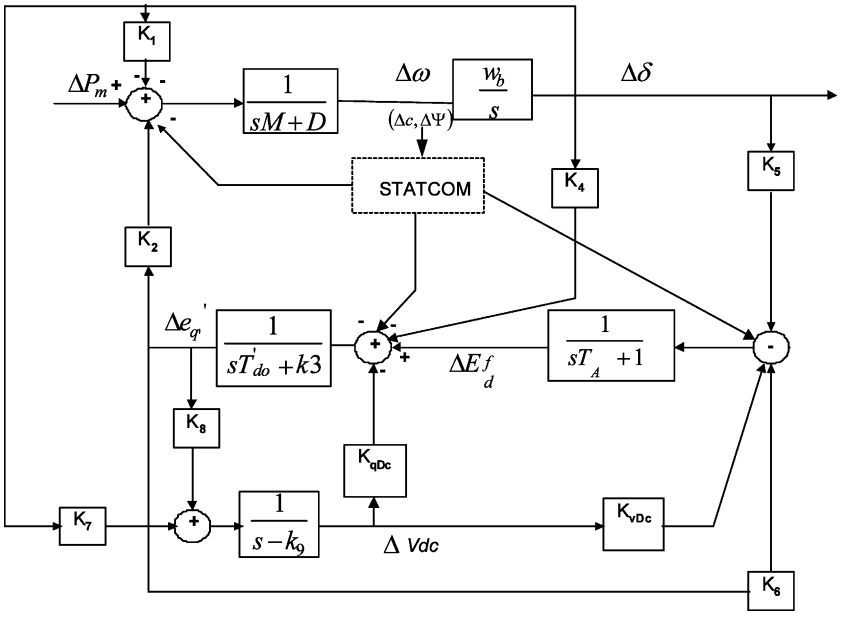

Fig. 2. The linearized system block diagram.

function, resulting from the variations in operating conditions, can be expressed in the form [16]

$$\tilde{P} = (1 + \Omega W_2)P \tag{7}$$

Here, W_2 is a fixed stable transfer function, also called the weight, and Ω is a variable transfer function satisfying $||\Omega||_\infty < 1$. The infinity norm (∞-norm) of a function is the least upper bound of its absolute value, also written as $||\Omega||_\infty = \sup_\omega |\Omega(j\omega)|$, is the largest value of gain on a Bode magnitude plot.

The plant transfer function is obtained from Eq. (6) as $P = H[\mathrm{sI} - \mathrm{A}]^{-1}\mathrm{B}$. The matrices A and B are operating point dependent through the coefficients K_1, K_2, etc. given in Appendix B. The uncertainties, which are the variations of system operating conditions, are thus modeled through $\tilde{P}$ in Eq. (7).

In the multiplicative uncertainty model Eq. (7), ΩW_2 is the normalized plant perturbation away from 1. If $||\Omega||_\infty < 1$, then

$$\left|\frac{\tilde{P(j\omega)}}{P(j\omega)} - 1\right| \le |W_2(j\omega j|, \ \forall\omega \tag{8}$$

So, $|W_2(j\omega)|$ provides the uncertainty profile, and in the frequency plane is the upper boundary of all the normalized plant transfer functions away from 1.

3.2. Robust stability and performance

Consider a multi-input control system given in Fig. 3. A controller C provides stability if it provides internal stability for every plant in the uncertainty set $\mathscr{P}$. If L denotes the open-loop transfer function ($L = PC$), then the sensitivity function S is written as

$$S = \frac{1}{1 + L} \tag{9}$$

The complimentary sensitivity function or the input–output transfer function is

$$T = 1 - S = \frac{PC}{1 + PC} \tag{10}$$

For a multiplicative perturbation model, robust stability condition is met if and only if $||W_2T||_\infty < 1$ [16,17]. This implies that

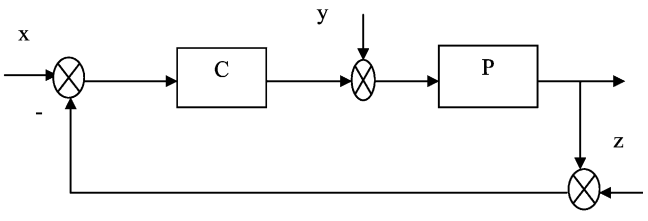

Fig. 3. Unity feedback plant with controller.

$$\left|\frac{W_2(j\omega)L(j\omega)}{1 + L(j\omega)}\right| < 1, \quad \text{for all } \omega \tag{11}$$

or,

$$|\Omega(j\omega)W_2(j\omega)L(j\omega)| < |1 + L(j\omega)|, \quad \text{for all } \omega, \text{ and } ||\Omega||_\infty < 1. \tag{12}$$

The block diagram of a typical perturbed system, ignoring all inputs, is shown in Fig. 4(a). The transfer function from output of Ω to the input of Ω equals $-W_2T$. The properties of the block diagram can be reduced to those of the configuration given in Fig. 4(b) [17,18].

The maximum loop gain $||-W_2T||_\infty$ is less than 1 for all allowable Ω if and only if the small gain condition $||W_2T||_\infty < 1$ holds. The nominal performance condition for an internally stable system is given as $||W_1S||_\infty < 1$, where W_1 is a real-rational, stable, minimum phase transfer function, also called a weighting function. If P is perturbed to $\tilde{P} = (1 + \Omega W_2)P$, S is perturbed to

$$\tilde{S} = \frac{1}{1 + (1 + \Omega W_2 L)} = \frac{S}{1 + \Omega W_2 T} \tag{13}$$

The robust performance condition should therefore be

$$\|W_2T\|_\infty < 1, \text{ and } \left\|\frac{W_1S}{1 + \Omega W_2 T}\right\| < 1, \quad \forall\|\Omega\| < 1. \tag{14}$$

Combining all the above, it can be shown that a necessary and a sufficient condition for robust stability and performance is [16]

$$\||W_1S| + |W_2T|\|_\infty < 1 \tag{15}$$

3.3. The loop-shaping technique

Loop shaping is a graphical procedure to design a proper controller C satisfying robust stability and performance criteria given above. The basic idea of the method is to construct the loop transfer function L to satisfy the robust performance criterion approximately, and then to obtain the controller from the relationship $C = L/P$. Internal stability of the plants and properness of C constitute the constraints of the method. Condition on L is such that PC should not have any pole zero cancellation.

A necessary condition for robustness is that either or both $|W_1|$ and $|W_2|$ must be less than 1 [16]. If we select a monotonically decreasing W_1 satisfying the other constraints on it, it can be shown that at low frequency the open-loop transfer function L should satisfy

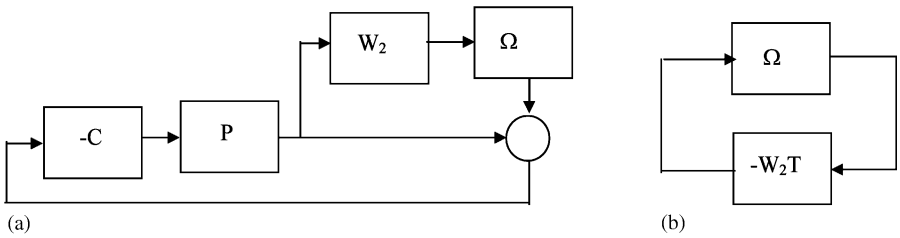

Fig. 4. (a) Feedback loop with uncertainty representation; (b) feedback loop in standard reduced form.

$$|L| > \frac{|W_1|}{1 - |W_2|} \tag{16}$$

while, for high frequency

$$|L| < \frac{1 - |W_1|}{|W_2|} \approx \frac{1}{|W_2|} \tag{17}$$

At high frequency $|L|$ should roll-off at least as quickly as $|P|$ does. This ensures properness of C. The general features of open-loop transfer function is that the gain at low frequency should be large enough, and $|L|$ should not drop-off too quickly near the crossover frequency resulting into internal instability.

3.4. The algorithm

The algorithm to generate a control transfer function C so that robust stability and robust performance conditions are met involves the following steps.

1) Obtain the dB-magnitude plot for the nominal as well as perturbed plant transfer functions.
2) Construct W_2 satisfying constraint Eq. (8).
3) Select W_1 as a monotonically decreasing, real, rational and stable function.
4) Choose L such that it satisfies conditions Eqs. (16) and (17). The transition at crossover frequency should not be at a slope steeper than -20 dB/decade. Nominal internal stability is achieved if on a Nyquist plot of L, the angle of L at crossover is greater than 180°.
5) Check for the nominal and robust performance criteria given in Section 3.2.
6) Construct the controller transfer function from the relation $C = L/P$.
7) Test for internal stability by direct simulation of the closed-loop transfer function for pre-selected disturbance or input.
8) Repeat steps 4 through 7 until satisfactory L and C are obtained.

4. STATCOM voltage controller implementation

The robust controller design procedure starts by arranging the system in the form shown in Fig. 3. The plant output to be fed back to the controller C is chosen to be the generator angular speed variation, $\Delta\omega$. The nominal operating point for the design was computed for a delivered power of 0.9 pu at unity power factor. The system parameters are given in Appendix C.

The nominal plant transfer function for the selected operating point is computed as

$$P = \frac{0.2104s^2(s + 100.827)(s - 0.234)}{(s + 99.1725)(s + 1.0945)(s + 0.0476)(s^2 + 0.6754s + 21.6344)} \tag{18}$$

Off-nominal power outputs between 0.4 and 1.4 pu and power factor from 0.8 lagging to 0.8 leading were considered. The dB-magnitude vs. frequency response for the nominal and perturbed plants is shown in Fig. 5.

From Fig. 5, the quantity, $|\tilde{P}(j\omega)/P(j\omega) - 1|$ for each perturbed plant is constructed and the uncertainty profile is fitted to the following function,

$$W_2(s) = \frac{0.9s^2 + 15s + 27}{s^2 + 5s + 31} \tag{19}$$

A Butterworth filter satisfies all the properties for $W_1(s)$ and is written as

$$W_1(s) = \frac{K_d f_c^2}{s^3 + 2s^2 f_c + 2s f_c{}^2 + f_c^3} \tag{20}$$

For $K_d = 0.01$ and $f_c = 0.1$, and for a choice of open-loop transfer function L as

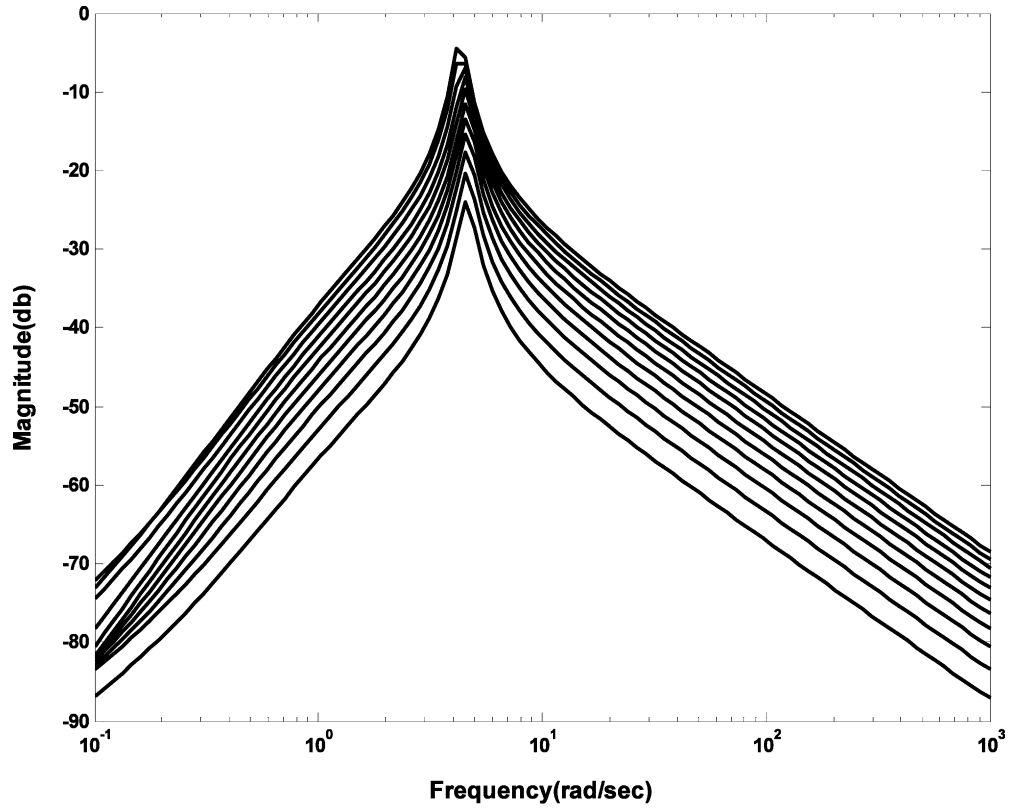

Fig. 5. dB-magnitude plot for nominal and perturbed plant transfer functions.

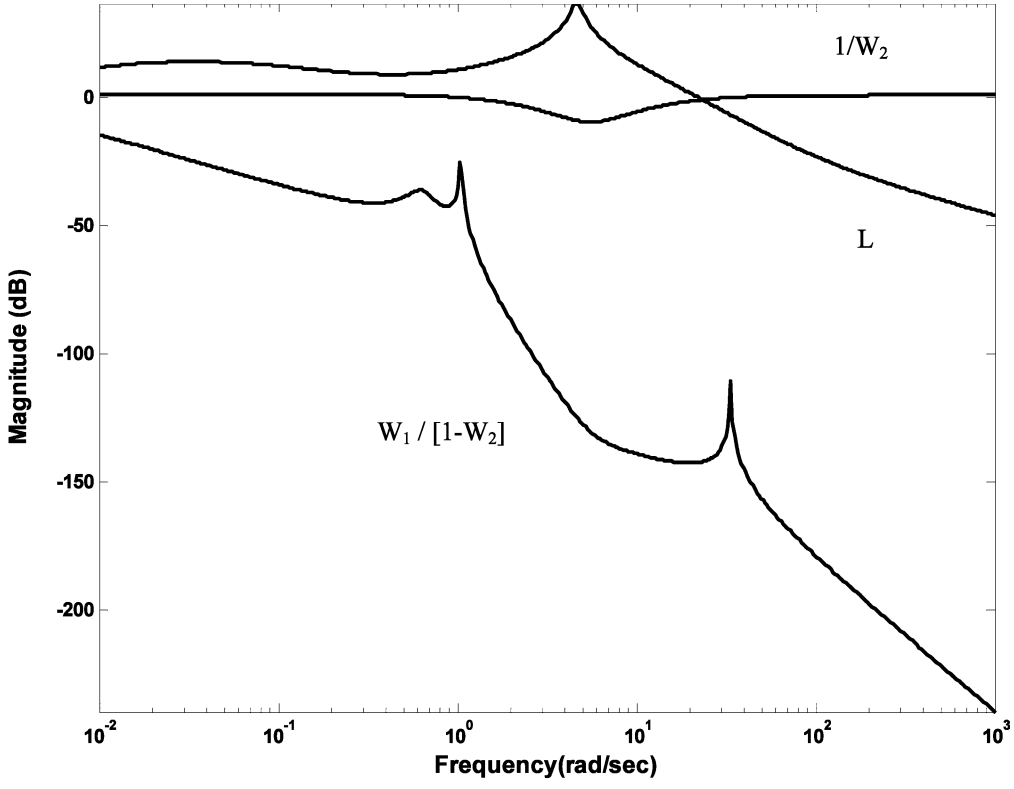

Fig. 6. Loop-shaping plots relating W_1, W_2 and L.

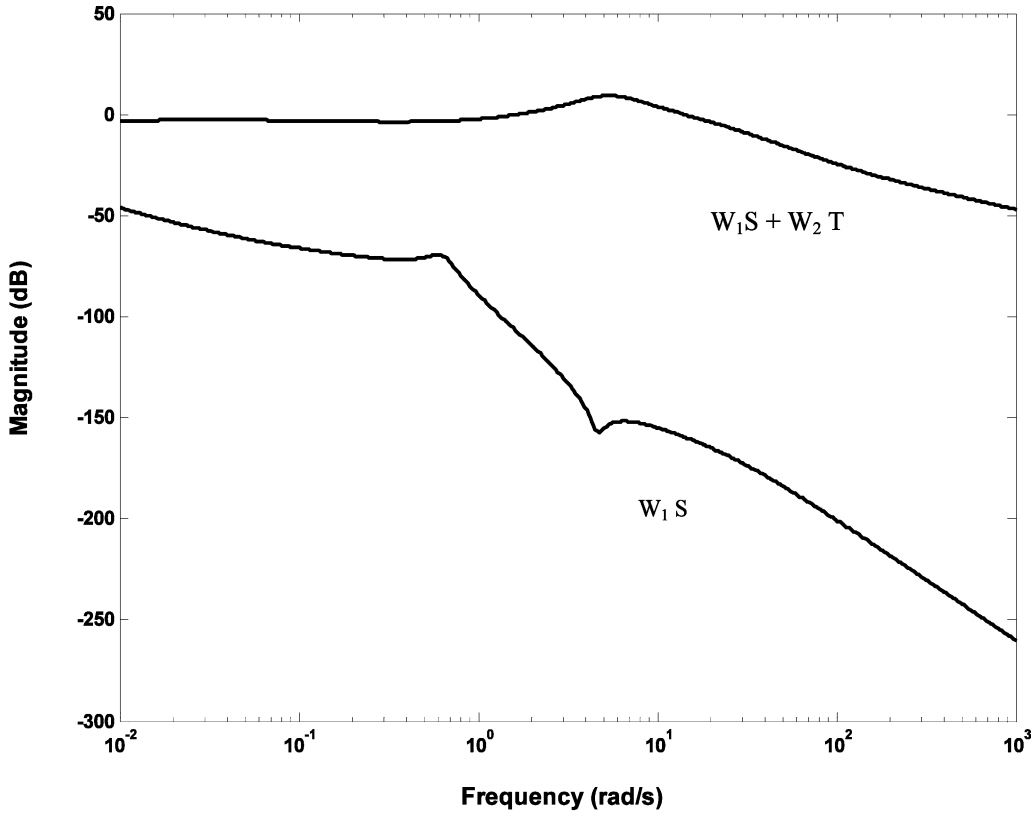

Fig. 7. The nominal and robust performance criteria.

$$L = \frac{5(s + 100.83)(s - 0.214309)(s + 1)(s + 0.001)}{(s + 10)(s + 0.1)(s + 0.01)(s^2 + 0.6754s + 21.6344)} \tag{21}$$

gives the desired controller transfer function

$$C = \frac{27.7631(s + 1)(s + 1.094)(s + 0.0476)(s + 0.001)(s + 99.1725)}{s^2(s + 10)(s + 0.1)(s + 0.01)} \tag{22}$$

The dB-magnitude plots relating W_1, W_2 and L, which were employed to arrive at this controller, is shown in Fig. 6. The open-loop function L is selected to fit the bounds set by Eqs. (16) and (17). The plots for the nominal and robust performance criteria are shown in Fig. 7. While the nominal performance measure W_1S is well-satisfied, the combined robust stability and performance measure has a small peak. This is because worst-case, zero damping condition was considered in the design.

Once the robust stability and performance criteria plotted in Fig. 7 are met, the stability and performance of the closed-loop system have to be checked by direct simulation of the system dynamic equations. MATLAB ODE routines were used for this purpose and the system was disturbed by a 50% input torque pulse for 0.1 s. Fine tuning on the controller parameters were performed from observation of the transient response of the system. Figs. 8–10 show the variations of generator angle, angular speed and STATCOM d.c. voltage variations, respectively, for the nominal plant, with and without control. Variation of the STATCOM d.c. voltage is very small thus enabling it to control both the reactive and real flow effectively (note, $V_{dco} = 4$ pu).

The effectiveness of the robust design was tested for a number of other operating conditions. Figs. 11 and 12 show the variations of generator rotor angle and the STATCOM d.c. voltage variations for the following four operating conditions: (a) 1.2-pu generator power output, 0.98-pf lead, (b) 1-pu output, 0.95 pf lag, (c) 0.9-pu output, unity pf and (d) 0.5-pu output, 0.95-pf lag.

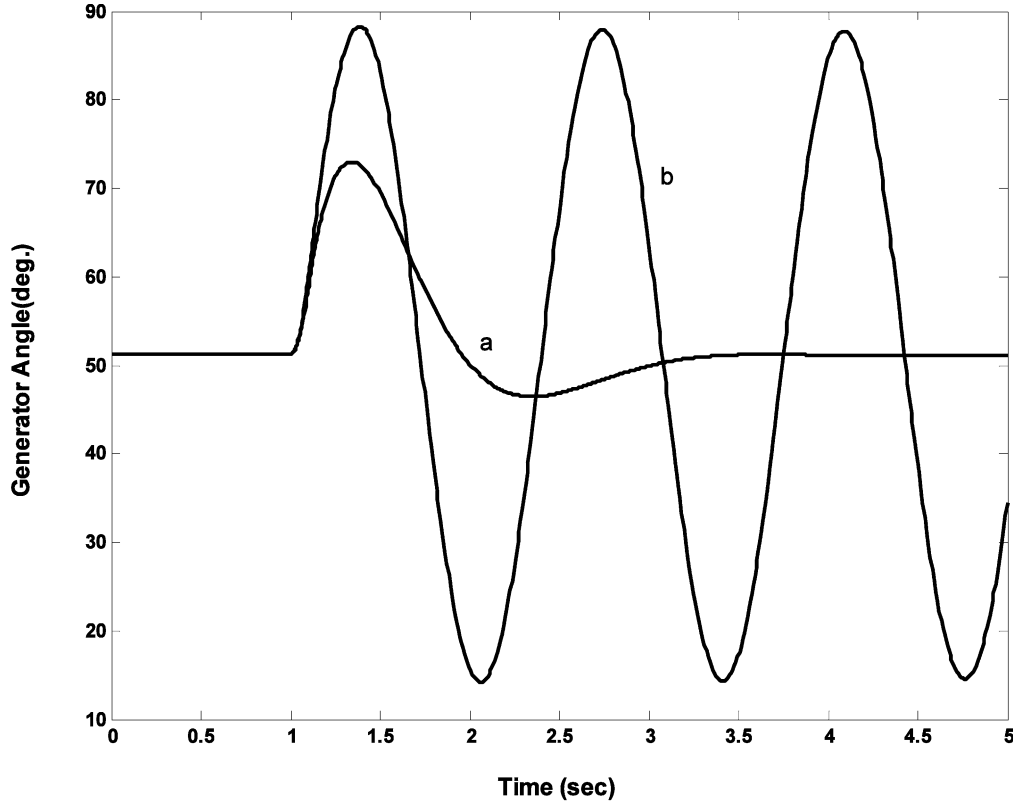

Fig. 8. Rotor angle variation following 50% input torque pulse for 0.1 s with (a) proposed robust control; and (b) no control.

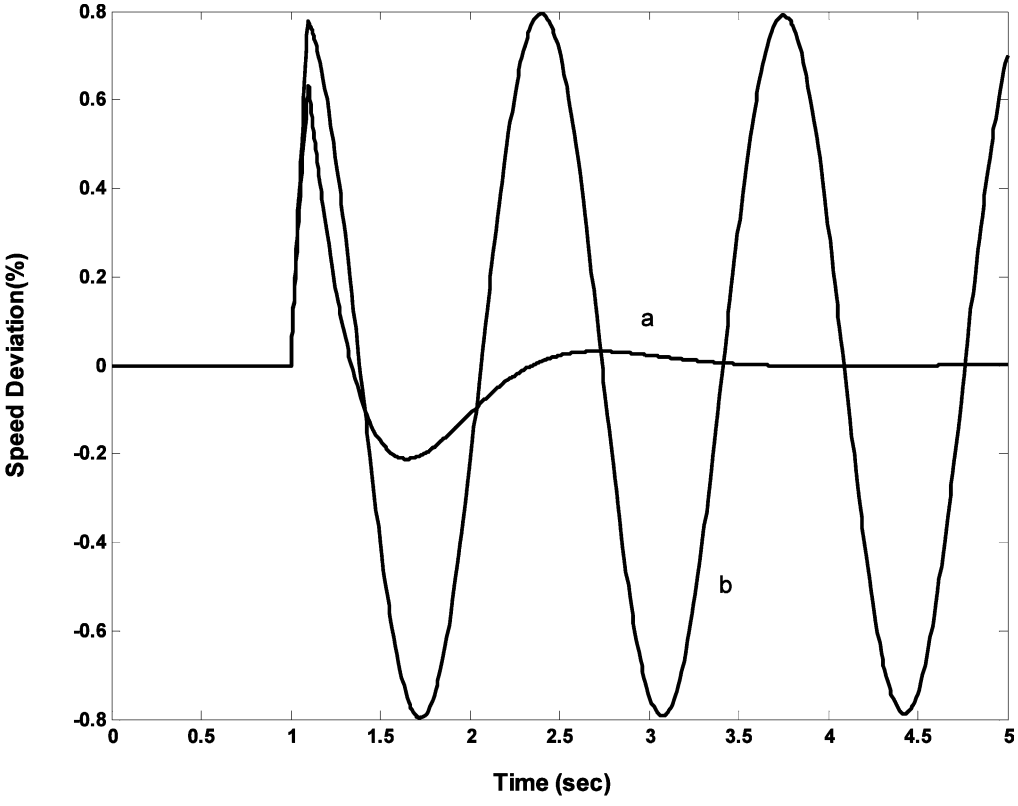

Fig. 9. Generator angular frequency variation corresponding to Fig. 8 with, (a) robust control; and (b) no control.

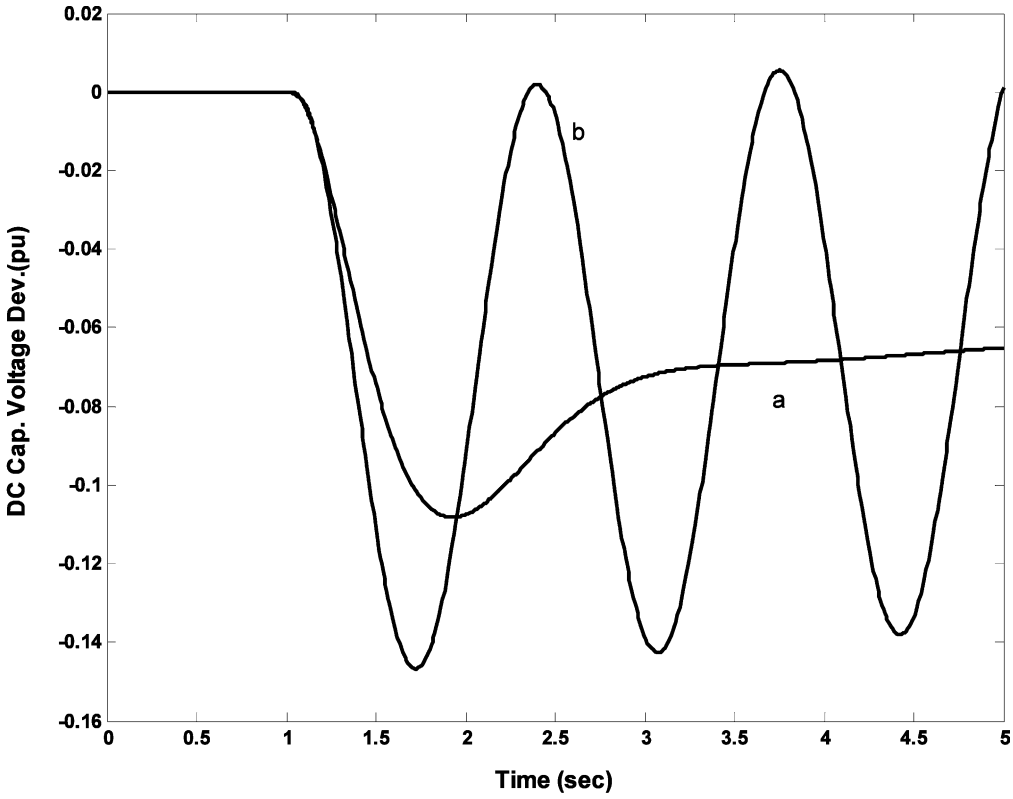

Fig. 10. D.C. capacitor voltage variation corresponding to the disturbance condition of Fig. 8 with, (a) robust control; and (b) no control.

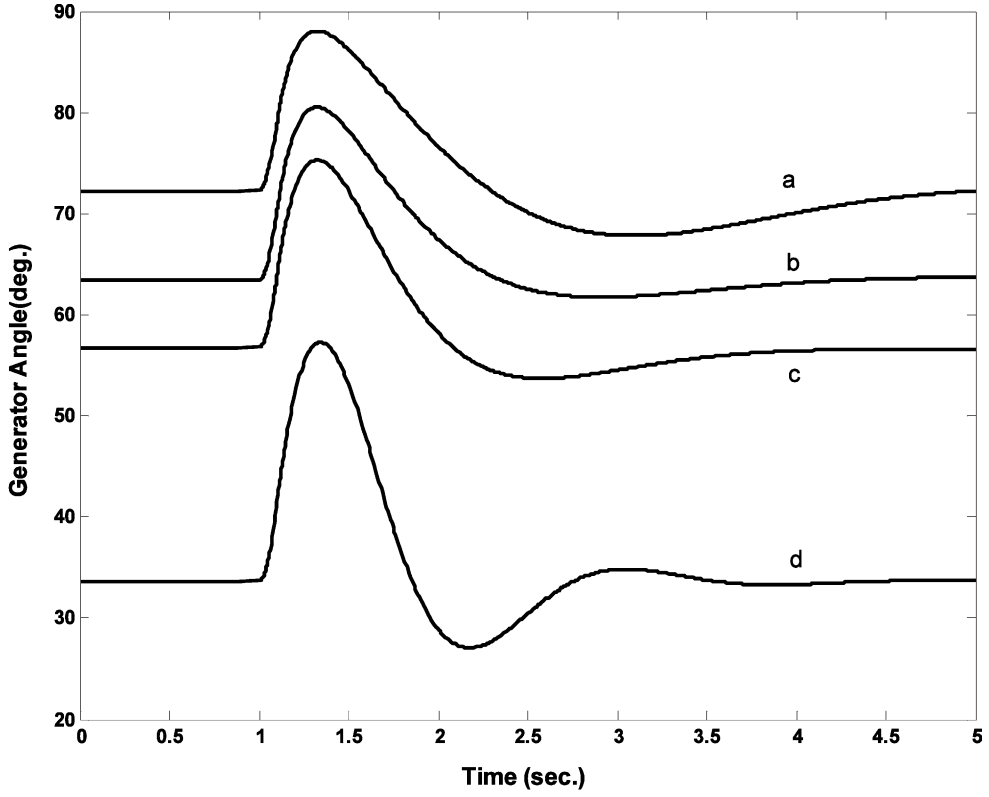

Fig. 11. Generator angle variations following 50% input torque pulse for 0.1 s, for (a) 1.2 pu power output, (b) 1 pu output, (c) 0.9 pu output, and (d) 0.5 pu output.

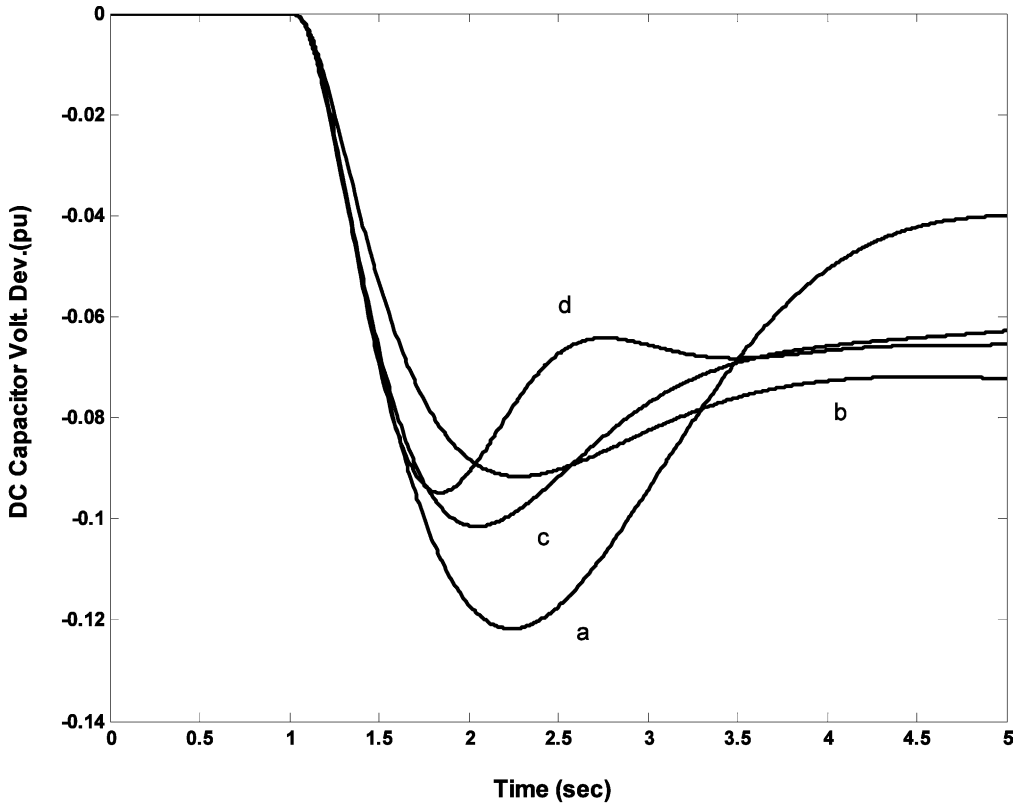

Fig. 12. D.C. capacitor voltage variations for the different load conditions corresponding to Fig. 11.

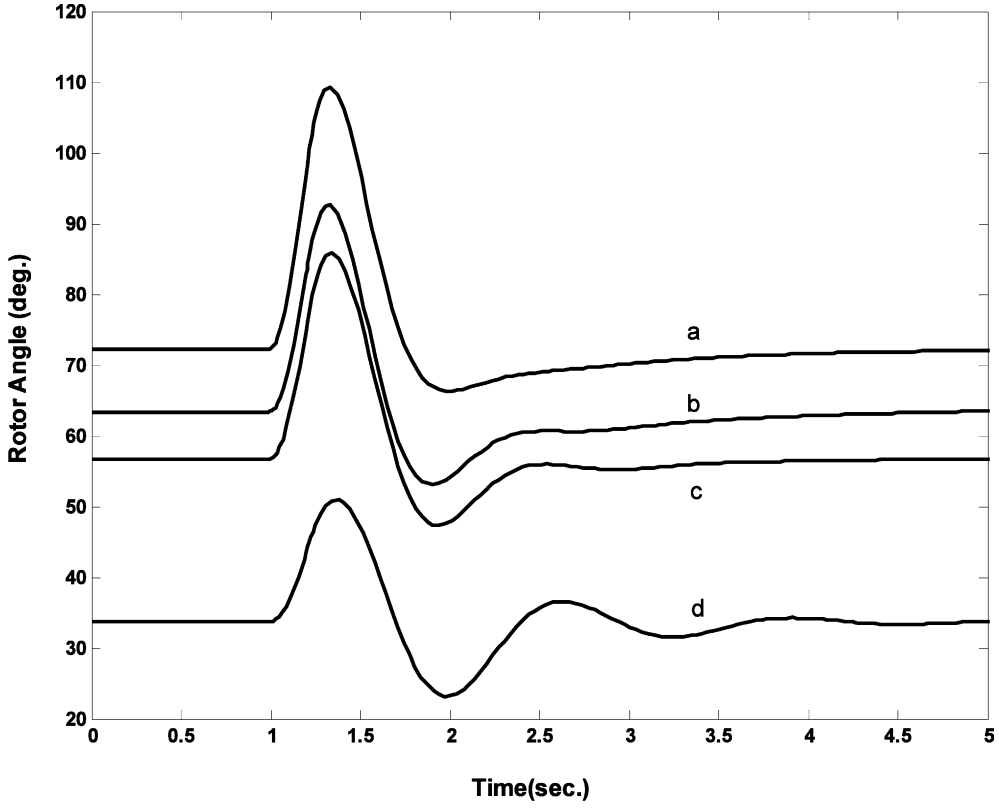

Fig. 13. Generator rotor angle variation following a three-phase fault on the remote bus for 0.1 s with, (a) 1.2 pu power output; (b) 1 pu output; (c) 0.9 pu output and; (d) 0.5 pu output.

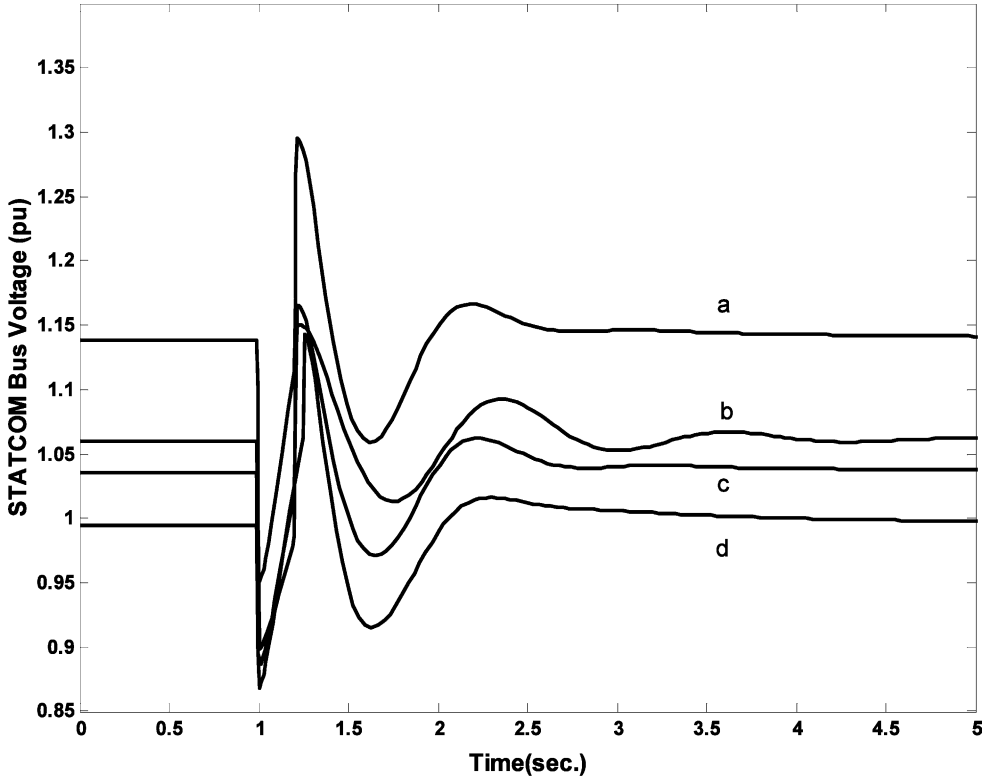

Fig. 14. STATCOM bus voltage variations following the three-phase fault condition of Fig. 13.

The disturbance considered in each case was a 50% torque pulse on the generator shaft for 0.1-s duration. It can be observed that the proposed controller is very effective in providing damping for such varying load conditions. Expectedly, the effectiveness of the controller will decrease as the point of operation moves further and further away from the nominal value.

The robust controller designed was also tested considering large disturbances. The nonlinear system of equations (5) was considered for this purpose. A three-phase fault for 0.1-s duration was simulated on the remote bus. The transient responses recorded for the generator rotor angle and STATCOM bus voltage variations for the four system operating conditions are shown in Figs. 13 and 14, respectively. Results show that the robust control damps both the electromechanical and electrical transients vary effectively. The controller can stabilize the unstable system for even longer fault durations. The transient voltage variations, however, are large in such cases.

5. Evaluation of the robust design

This section presents a comparison of the responses obtained by the proposed H_∞-based robust controller design with fixed parameter controllers. Optimum fixed parameter controller may be designed using linear regulator formulation, PID controller tuning based on pole-placement technique, etc. These methods produce optimum controller functions for linear systems designed for specific operating points. We consider the pole-placement method to design the gains of a PID controller in the following.

Consider a PID controller,

$$G_{\mathrm{PID}}(s) = K_{\mathrm{P}} + \frac{K_{\mathrm{I}}}{s} + K_{\mathrm{D}}s \tag{23}$$

Here, K_{P}, K_{I}, K_{D} are the gains in the proportional, integral and derivative loops. Often a washout has to be included in the controller to eliminate any unwanted steady state signal. The controller transfer function then takes the form

$$G_{\mathrm{c}}(s) = \frac{sT_{\mathrm{w}}}{1 + sT_{\mathrm{w}}}\left(K_{\mathrm{P}} + \frac{K_{\mathrm{I}}}{s} + K_{\mathrm{D}}s\right) \tag{24}$$

where T_{w} is the washout time constant.

By assigning three poles of the compensated closed-loop system the appropriate values of K_{P}, K_{I} and K_{D} can be determined. The location of the dominant eigenvalues can be selected to provide the specified damping to the system. For the choice of dominant eigenvalues at $-3 \pm j10$, corresponding to the damping ratio of 0.287,

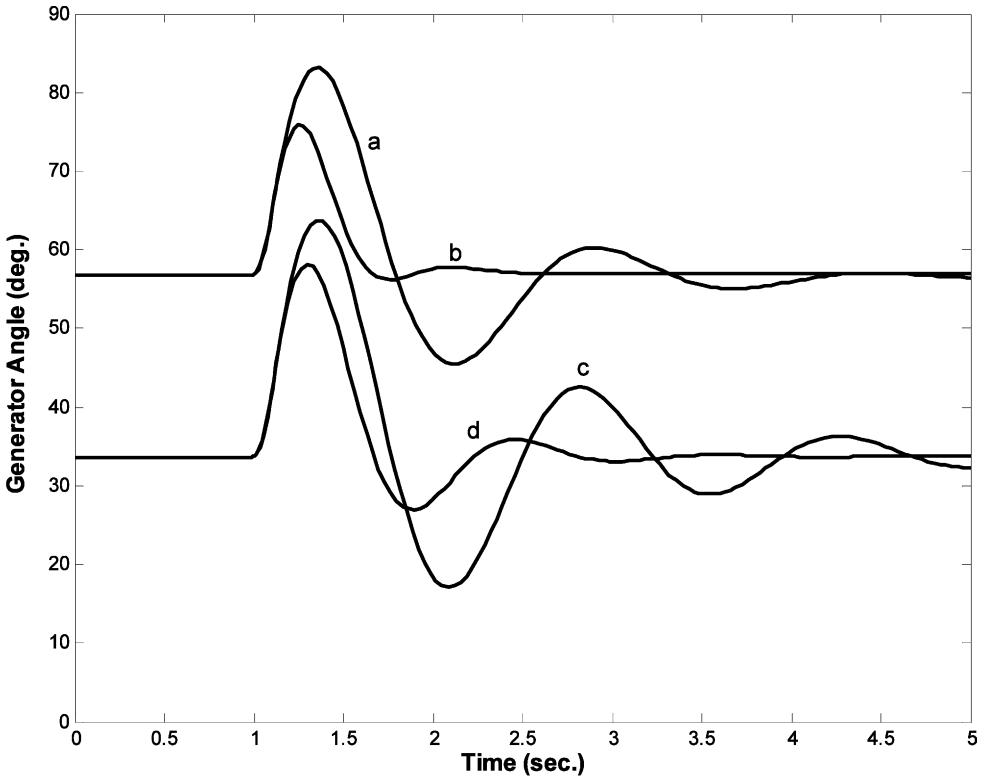

Fig. 15. Comparison of rotor angle characteristics with PID and robust controllers—at nominal loading (a) PID control; (b) robust control; at 0.5 loading; (c) PID control; (d) robust control.

the PID controller gains at the nominal operating point were obtained as

$$K_P = 5.4928$$
$$K_I = 2.18409 \quad (25)$$
$$K_D = 3.2166$$

The location of a third root is maintained at -1.091 before and after compensation. The theory for the pole-placement method is available in the literature [19].

Fig. 15 gives a comparison of the rotor angle variations for a 50% input torque pulse for 0.1 s. Curves 'a' and 'b' show the responses with the PID and robust controls, respectively, at the nominal loading. It can be observed that the response with the robust design is superior to the PID design. Curves 'c' and 'd' are the responses with PID and robust controls, respectively, at 0.5-pu loading and 0.95 lagging power factor. The set of values in Eq. (25) obtained for the nominal operating condition was used in the simulation. From the transient response, it is clear that the gain settings have to be recalculated to give satisfactory transient response. The robust controller, however, performs well at this operating point that is quite far from the nominal one.

6. Conclusion

A simple method of designing robust damping controller for a power system through control of STATCOM voltage magnitude is proposed. The design is carried out employing both robust stability and robust performance considerations. Fixed-gain constant-coefficient controller transfer function in the s-domain was obtained which provide robust damping characteristics through a graphical loop-shaping technique. A detailed generator model having a voltage controlled STATCOM was considered. The controller was tested for a number of disturbance conditions including symmetrical three-phase faults. The robust design has been found to be very effective for a range of operating conditions of the power system. The loop-shaping method utilized to determine the robust controller function is simple and straightforward to implement.

The design employed a nominal power output of 0.9 pu at unity power factor, and the perturbations in the range of 0.4–1.4 pu. The controller design provides excellent damping control in the vicinity of nominal loading. For operation of the power system at extreme light or heavy loads and for leading power factor conditions, switching to other control functions may be necessary. However, the controller function pre-

sented here will cover the normal loading ranges of the system.

Acknowledgements

The authors wish to acknowledge the facilities provided at the King Fahd University of Petroleum and Minerals, Dhahran, Saudi Arabia.

Appendix A: Nomenclature

X_{TL}, X_{LB}	transmission line reactances
M, D	inertia and damping coefficients
V_t	generator terminal voltage
P_m, P_e	generator input and output power
C_{dc}	d.c. capacitance
ψ	phase angle of the mid-bus voltage
e_q', e_q	internal voltage behind transient and synchronous reactances
E_{fd}	generator field voltage
δ	generator rotor angle
T_{do}'	open circuit field time constant
K_A, T_A	exciter gain and time constants
x_d, x_d'	direct axis synchronous and transient reactance
ω_0	base radian frequency
i_d, i_q	armature currents along d–q axes
V_d, V_q	armature voltage in d–q axes
V_b, V_m	infinite bus and STATCOM bus voltages

Appendix B: The linearized system equations

Taking variations around the operating points, Eq. (3) can be written as

$$\Delta\dot{\delta} = \omega_0\Delta\omega$$
$$\Delta\dot{\omega} = -\frac{1}{M}[-\Delta P_e - D\Delta\omega]$$
$$\dot{\Delta e}_q' = \frac{1}{T_{do}'}[-\Delta e_q' + \Delta E_{fd} - (x_d - x_d')\Delta I_{tLd}]$$
$$\dot{\Delta E}_{fd} = -\frac{1}{T_A}(\Delta E_{fd} - K_A\Delta V_t)$$
$$\dot{\Delta V}_{dc} = \frac{1}{C_{Dc}}\begin{bmatrix}(I_{Lod}\cos\psi_0 + I_{Loq}\sin\psi_0)\Delta m \\ +m_0(-I_{Lod}\sin\psi_0 + I_{Loq}\cos\psi_0)\Delta\psi + \\ +m_0(\cos\psi_0\,\Delta I_{Lod} + \Delta I_{Loq}\sin\psi_0)\end{bmatrix} \tag{A1}$$

$\Delta\omega$ represents the per unit speed and is given as $(\omega - \omega_0)/\omega_0$. The perturbations of the non-state variables Eq. (4) are

$$\begin{aligned}\Delta P_e &= K_1\Delta\delta + K_2\Delta e_q' + K_{pDc}\Delta V_{Dc} + K_{pe}\Delta m + K_{p\psi}\Delta\psi \\ \Delta e_q &= K_4\Delta\delta + K_3\Delta e_q' + K_{qDc}\Delta V_{Dc} + K_{qe}\Delta m + K_{q\psi}\Delta\psi \\ \Delta V_t &= K_5\Delta\delta + K_6\Delta e_q' + K_{vDc}\Delta V_{Dc} + K_{ve}\Delta m + K_{v\psi}\Delta\psi\end{aligned} \tag{A2}$$

The state matrix can be written as,

$$\begin{bmatrix}\dot{\Delta\delta}\\ \dot{\Delta\omega}\\ \dot{\Delta eq'}\\ \dot{\Delta E}_{fd}\\ \dot{\Delta V}_{dc}\end{bmatrix} = \begin{bmatrix}0 & \omega_b & 0 & 0 & 0\\ -\frac{K_1}{M} & -\frac{D}{M} & -\frac{K_2}{M} & 0 & -\frac{K_{pdc}}{M}\\ -\frac{K_4}{T_{do'}} & 0 & -\frac{K_3}{T_{do'}} & -\frac{1}{T_{do'}} & -\frac{K_{qdc}}{T_{do'}}\\ -\frac{K_AK_5}{T_A} & 0 & -\frac{K_AK_6}{T_A} & -\frac{1}{T_A} & -\frac{K_AK_{vdc}}{T_A}\\ K_7 & 0 & K_8 & K_9 & 0\end{bmatrix} \times \begin{bmatrix}\Delta\delta\\ \Delta\omega\\ \Delta eq'\\ \Delta E_{fd}\\ \Delta V_{dc}\end{bmatrix} + \begin{bmatrix}0 & 0\\ -\frac{K_{pc}}{M} & -\frac{K_{q\Psi}}{M}\\ -\frac{K_{qc}}{T_{do'}} & -\frac{K_{q\Psi}}{T_{do'}}\\ -\frac{K_AK_{vC}}{T_A} & -\frac{K_AK_{v\Psi}}{T_A}\\ K_{dc} & K_{d\Psi}\end{bmatrix}\begin{bmatrix}\Delta m\\ \Delta\Psi\end{bmatrix} \tag{A3}$$

Appendix C: The system parameters

All the quantities are in per unit, except as indicated. $H = 3.0$ s, $T_{do}' = 6.3$ s, $x_d = 1.0$, $x_d' = 0.3$, $x_q = 0.6$, $D = 0$; $X_{TL} = 0.3$, $X_{LB} = 0.3$, $X_{SDT} = 0.15$, $K_A = 10$, $T_A = 0.05$ s, $C_{dc} = 1.0$, $m_0 = 0.25$, $\psi_0 = 46.52^\circ$.

Nominal plant operating conditions: $P_{eo} = 0.9$, $V_{to} = 1.0$, pf $= 1.0$.

References

[1] L. Gyugyi, Dynamic compensation of ac transmission lines by solid-state synchronous voltage sources, IEEE Trans. Power Delivery 9 (2) (1994) 904–911.
[2] J. Machowski, Power System Dynamics and Stability, Wiley, 1997.
[3] N. Hingorani, L. Gyugi, Understanding FACTS, IEEE Press, New York, 2000.
[4] C. Li, Q. Jiang, Z. Wang, D. Retzmann, Design of a rule based controller for STATCOM, Proceedings of the 24th Annual Conference of IEEE Ind. Electronic Society, IECon '98, vol. 1, 1998, pp. 467–472.
[5] H.F. Wang, F. Li, Design of STATCOM multivariable sampled regulator, International Conference on Electric Utility Deregulation and Power Technology 2000, City University, London, April, 2000.

[6] H. Wang, F. Li, Multivariable sampled regulators for the co-coordinated control of STATCOM ac and dc voltage, IEE Proc.—Generation Transm. Distrib. 147 (2) (2000) 93–98.
[7] K.R. Padiyar, A.L. Devi, Control and simulation of static condenser, APEC 94—Ninth Annual Applied Power Electronics Conference and Exposition, vol. 1, no. 2, 1994, pp. 826–831.
[8] H.F. Wang, Phillips-Heffron model of power systems installed with STATCOM and applications, IEE Proc. Generation Transm. Distrib. 146 (5) (1999) 521–527.
[9] P. Rao, M.L. Crow, Z. Young, STATCOM control for power system voltage control applications, IEEE Trans. Power Delivery 15 (2000) 1311–1317.
[10] P.S. Sensarma, K.R. Padiyar, V. Ramnarayanan, Analysis and performance evaluation of a distribution STATCOM for compensating voltage fluctuation, IEEE Trans. Power Delivery 16 (2001) 259–264.
[11] K.V. Patil, J. Senthil, J. Jiang, R.M. Mathur, Application of STATCOM for damping torsional oscillations in series compensated ac systems, IEEE Trans. Energy Convers. 13 (3) (1998) 237–243.
[12] P.W.D.S. Lehn, Modeling, analysis and control of current source inverter based STATCOM, IEEE Trans. Power Delivery 17 (2002) 248–253.
[13] M.M. Farasangi, Y.H. Song, Y.Z. Sun, Supplementary control design of SVC and STATCOM using H_∞ optimal robust control, Proceedings of the International Conference on Electric Utility Deregulation 2000, City University London, April, 2000, pp. 355–360.
[14] H. Chen, R. Zhou, Y. Wang, Analysis of voltage stability enhancement by robust nonlinear STATCOM control, Proceedings of the IEEE PES Summer Meeting, 2000, vol. 3, pp. 1924–1929.
[15] A.H.M.A. Rahim, S.A. Al-Baiyat, H.M. Al-Maghrabi, Robust damping controller design for a static compensator, IEE Proc.—Generation Transm. Distrib. 149 (4) (2002) 491–496.
[16] J.C. Doyle, B.A. Francis, A.R. Tannenbaum, Feedback Control Theory, MacMillan Publishing Co, New York, 1992.
[17] A. Chao, M. Athans, Stability robustness to unstructured uncertainty for linear time invariant systems, in: W.S. Levine (Ed.), The Control Handbook, CRC Press and IEEE Press, 1996.
[18] M.A. Dahleh, l_1 Robust control: theory, computation and design, in: W.S. Levine (Ed.), The Control Handbook, CRC Press and IEEE Press, 1996.
[19] Y. Hsu, C. Chen, Tuning of power system stabilizers using an artificial neural network, IEE Trans. Energy Convers. 6 (4) (1991) 612–619.